Microstructural analysis of TRISO particles using multi-scale X-ray computed tomography

Journal of Nuclear Materials 461 (2015) 29–36

Contents lists available at ScienceDirect

Journal of Nuclear Materials

journal homepage: www.elsevier.com/locate/jnucmat

Microstructural analysis of TRISO particles using multi-scale X-ray computed tomography

T. Lowe [a,*], R.S. Bradley [a], S. Yue [a,d], K. Barii [b], J. Gelb [c], N. Rohbeck [a], J. Turner [b], P.J. Withers [a,d]

[a] Manchester X-ray Imaging Facility, School of Materials, University of Manchester, M13 9PL, UK
[b] School of Mechanical Engineering, University of Manchester, M13 9PL, UK
[c] Zeiss Xradia Inc., Pleasanton, CA, USA
[d] The Research Complex at Harwell, Rutherford Appleton Laboratory, Didcot, Oxfordshire OX11 0FA, UK

ARTICLE INFO

Article history:
Received 21 November 2014
Accepted 20 February 2015
Available online 28 February 2015

ABSTRACT

TRISO particles, a composite nuclear fuel built up by ceramic and graphitic layers, have outstanding high temperature resistance. TRISO fuel is the key technology for High Temperature Reactors (HTRs) and the Generation IV Very High Temperature Reactor (VHTR) variant. TRISO offers unparalleled containment of fission products and is extremely robust during accident conditions. An understanding of the thermal performance and mechanical properties of TRISO fuel requires a detailed knowledge of pore sizes, their distribution and interconnectivity. Here 50 nm, nano-, and 1 μm resolution, micro-computed tomography (CT), have been used to quantify non-destructively porosity of a surrogate TRISO particle at the 0.3–10 μm and 3–100 μm scales respectively. This indicates that pore distributions can reliably be measured down to a size approximately 3 times the pixel size which is consistent with the segmentation process. Direct comparison with Scanning Electron Microscopy (SEM) sections indicates that destructive sectioning can introduce significant levels of coarse damage, especially in the pyrolytic carbon layers. Further comparative work is required to identify means of minimizing such damage for SEM studies. Finally since it is non-destructive, multi-scale time-lapse X-ray CT opens the possibility of intermittently tracking the degradation of TRISO structure under thermal cycles or radiation conditions in order to validate models of degradation such as kernel movement. X-ray CT in-situ experimentation of TRISO particles under load and temperature could also be used to understand the internal changes that occur in the particles under accident conditions.

1. Introduction

Tri-structural-isotropic (TRISO) fuel particles are an integral part of the fuel design for current and future High Temperature Reactors (HTRs). They offer the prospect of excellent retention of fission products throughout service, and maintain this during severe accident conditions where temperatures can reach up to 1600 °C.

A TRISO particle comprises four concentric spherical layers encasing a fuel kernel, namely the buffer (porous carbon), inner pyrolytic carbon (IPyC), silicon carbide (SiC) and outer pyrolytic carbon (OPYC) layers. Each layer performs specific functions:

A. The fuel kernel consisting of uranium or uranium carbide provides the fissile material and retains some of the fission products.
B. The buffer layer, a highly porous carbon structure, provides some free volume for gaseous fission products, and protects the SiC layer from high energy fission product damage.
C. The IPyC layer provides structural support for the subsequent SiC layer and prevents the chlorine compounds required for SiC deposition interacting with the fuel kernel.
D. The SiC layer forms the main diffusion barrier for fission products. It acts as a pressure vessel providing mechanical strength for the particle during manufacture of the nuclear fuel compact or pebble bed.
E. The OPyC layer protects the SiC layer during fuel fabrication, as the TRISO particle is pressed into a larger fuel compact or pebble.

This study examines the applicability of multi-scale X-ray computed tomography (CT) for the non-destructive quantification of porosity and thickness of the various layers of TRISO particles in three dimensions and compares this to the current destructive method involving high resolution Scanning Electron Microscopy

* Corresponding author.
E-mail address: tristan.lowe@manchester.ac.uk (T. Lowe).

http://dx.doi.org/10.1016/j.jnucmat.2015.02.034
0022-3115/

(SEM) imaging of prepared cross sections. This comparison allows a direct assessment of the damage introduced to particles by the destructive sample preparation methods typically used for cross-sectional imaging. Furthermore, CT measurements are of sufficient quality to guide the optimization of manufacturing conditions and to provide 2D or 3D structural models for image-based numerical modelling of the thermal behaviour of the particles.

To date, the majority of TRISO particle studies have relied on SEM to characterize the microstructure of the layers [1–3]. However, this approach raises the possibility that the destructive sample preparation process introduces damage, particularly in the more porous layers. Furthermore 2D images may not capture the connectivity of porosity nor intersect key defects. This is especially true for the carbon layers which are known to be anisotropic. Hence the 3D characterization of the layers by X-ray CT potentially offers a distinct advantage. An added advantage of non-destructive techniques when looking at uranium containing particles is the containment of radioactive material by maintaining the integrity of the fuel particle.

Although Rochais et al. [4] have recently shown some success with synchrotron based CT of TRISO particles, synchrotron experiments are expensive to undertake and access to synchrotron facilities can be difficult to obtain restricting its widespread application. Consequently, a number of researchers [5,6] have developed laboratory based X-ray CT and radiography techniques for characterising the TRISO layer structure. Until recently these techniques have been hampered by significantly inferior spatial resolution, limiting the accuracy of the layer profiles that can be obtained. Unfortunately the polychromatic nature of laboratory-based X-ray sources also means that beam hardening artefacts [7] due to highly attenuating materials such as the TRISO kernel becomes an important factor. Although beam hardening can be reduced by increasing the average photon energy this in turn reduces the contrast difference between the subsequent buffer, IPyC, SiC and OPyC layers as well as pore features within the individual layers. At present most laboratory based X-ray CT instruments (worse than ~5 μm resolution) are unable to characterise the fine pore structures found in the TRISO layers. This has resulted in TRISO particles traditionally being characterised using SEM analysis of cross-sections despite the associated sample preparation issues.

2. Experimental

A set of 5 surrogate TRISO particle obtained from the Institute of Trans-Uranium Elements (ITU, Germany) was used to test the feasibility of XCT analysis. However in this study only one particle was fully analysed using 3D visualisation software for quantification as a "proof of concept". The particle was fabricated by fluidized bed chemical vapour deposition as described by López-Honorato et al. [1]. Using a zirconia (ZrO_2) sphere of 500 μm diameter as a non-radioactive surrogate for the uranium oxide kernel. The particle layers from inside to outside were Buffer, IPyC, SiC and OPyC.

The specimen was mounted on a thin polymer cylinder using an adhesive after which it was analysed using Xradia VersaXRM-500 and UltraXRM-L200 laboratory X-ray microscopes (Xradia, Inc., Pleasanton, CA, USA). The Xradia VersaXRM-500T was operated at 40 kV and 74 mA with a specimen to source distance of 45 mm and a specimen to detector distance of 9 mm. The whole TRISO particle could be viewed at 4× magnification at a voxel size of 0.56 μm (the pixel size and voxel size hold the same numerical value, the voxel size along each axis is used for the volume). The VersaXRM is capable of a 3D spatial resolution of 700 nm which is suitable for precisely separating the multiple layers within the sphere. The polychromatic imaging technique enabled high contrast on the low-Z outer shell layers, balanced with penetration through the ZrO_2 kernel. The UltraXRM-L200 employs a Cr target with characteristic radiation at 8.1 kV. It was operated in the lower magnification (150 nm) configuration, giving a 65 nm voxel size, with a 65 μm field of view. The Zernike phase contrast imaging mode was employed to enhance the contrast of features within the low-Z outer layer. A region of interest scan was conducted [8], enabling the outer layer to be imaged without destroying the sample. Consequently the structural integrity of the particle was maintained allowing for additional imaging with the higher resolution (50 nm) mode and, if desired, eventual destructive imaging.

The specimen was rotated over a 186° rotation range for the VersaXRM and 180° range for the UltraXRM, collecting 2401 and 1441 total images per scan respectively. After image acquisition, the data sets were loaded into the Xradia XMReconstructor software for reconstruction of the 3D virtual slices using filtered back projection.

The reconstructed data was then analysed using Avizo standard 7.0 (Visualization Sciences Group, Bordeaux (VSG), France) to segment and visualise the virtual slices and 3D volume renderings. For the Versa XRM datasets the porosity in the Buffer, IPyC and OPyC layers was segmented using the adaptive thresholding technique as described in Section 3.3. As the width of the pores is relatively narrow and pore morphology fairly consistent, a baseline image was created using a morphological closing filter (dilation followed by erosion of same kernel size). This process averages the grey scale values of neighbouring voxels so that the pores could be adaptively extracted by subtracting the original image from the filtered image resulting in a pore outline.

For the UltraXRM data, a simple thresholding technique based upon grey scale value was used to distinguish the porosity within the OPyC layer due to the lack of either beam hardening or partial volume effects.

For direct comparison with SEM analysis, the specimen was prepared using a traditional SEM method, whereby the TRISO particle was embedded in epoxy resin and ground using 1200 grade SiC paper. The grinding stage was followed by polishing on 6, 1 and 0.25 μm diamond paste media. The polished specimen was then coated with 5 nm of carbon using a Gatan Precision Etching and Coating System (PECS). The coated sample was observed in a FEI Quanta 650 field emission gun scanning electron microscope (FEGSEM) at an acceleration voltage of 20 keV. Images were taken in both secondary electron and backscattered electron modes; the latter showing atomic number contrast imaging where the higher atomic number elements (Si and Zr) are observed as brighter regions.

3. Results

3.1. Comparison of X-ray CT volumes with SEM images

The full layered structure of the TRISO particle can be seen in good contrast from the reconstructed orthoslices from the Versa (Fig. 1a). Visually, the porosity in the buffer (B) and OPyC (E) layers appears to be broadly similar to that revealed by SEM analysis (Fig. 1b) at a similar magnification. However a comparison between the two techniques highlights a number of differences, some of which are quantified in Table 1. SEM analysis of the IPyC layer (C) (Fig. 1c) reveals a number of small pores (<2 μm), many of which are situated close to the SiC interface (C–D), that are not seen in the CT images because they are near the resolution limit of the Versa X-ray CT. Given the hardness of the SiC material these small pores are unlikely to be caused by sample preparation. A major feature in the SiC layer for the SEM analysis is the large crack; however this can be attributed to sample preparation during

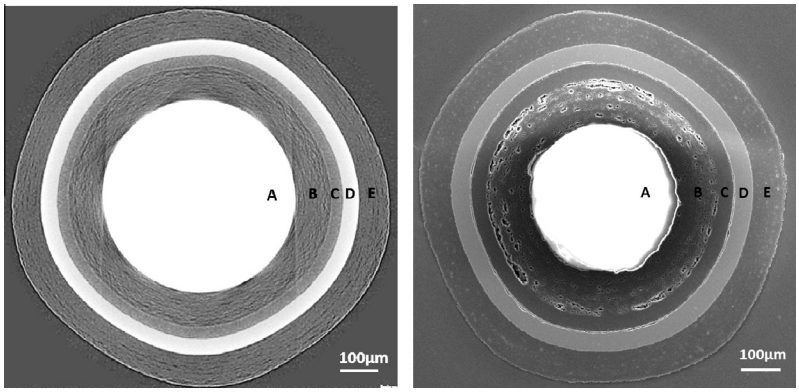

Fig. 1. (a) shows an orthoslice through the centre of a TRISO particle from a 3D volume acquired on the VersaXRM, (b) an SEM micrograph through the centre of a TRISO particle. **A** – Kernel, **B** – Buffer, **C** – IPyC, **D** – SiC and **E** – OPyC.

Table 1
The mean thickness for each layer (buffer, IPYC, SiC and OPYC) of the TRISO particle. The error associated with each layer was calculated from the standard deviation.

Material	Layer fractions	Mean layer thickness (µm)	Layer thickness standard deviation (µm)	Variation of layer thickness (µm)	Volume fraction of porosity in layer	Pore area fraction from single slice	Pore area fraction from SEM micrograph
Kernel (radius)	0.113	257.4	5.2	25	–	–	–
Buffer	0.207	94.1	3.9	20	2.9	0.0050	0.0100
IPYC	0.101	31.3	1.4	12	–	–	0.0014
SiC	0.159	41.1	0.8	6	–	–	0.0033
OPYC	0.440	77.9	4.6	30	2.4	0.0031	0.0047

grinding and polishing and as such is not expected in the X-ray CT results.

In the OPyC layer (E) both techniques show a similar pore type structure that appears to form in layers concentric to the sphere. A quantitative analysis of Fig. 1a and b using the Avizo visualisation software (Table 1) shows X-ray CT to give a slightly higher porosity content in this layer.

SEM and X-ray CT analysis deviate most significantly for the highly porous buffer layer (B). In the X-ray CT image (Fig. 2a) the pores appear along specific sub-layers within the layer. By contrast in the SEM micrograph (Fig. 2b) the pores are significantly larger with a much wider distribution in size. The difference in the pore morphology and porosity content (Table 1) can be attributed to the SEM specimen preparation, where the hard grinding medium results in particle pull-out damage from the soft, porous buffer material. Consequently the damage introduced by sample preparation explains the larger fraction of large pores observed by SEM. As regards the distribution of small pores it should be remembered that the segmentation process along with the spatial resolution of the CT system places a lower limit on the pores that can be observed by CT to around 2–3 µm.

These results suggest that CT vs SEM comparison studies are needed to develop standardised sample preparation procedures that limit the introduction of damage into SEM cross sections if this method is to be used as the primary way of characterising particle defects and structure.

3.2. Quantifying layer thicknesses

The thickness of TRISO particle layers is a function of several fabrication parameters. It can also be affected by in-service conditions, particularly neutron irradiation, and the extent of induced changes can be a significant factor in particle failure. Given the difficulties in determining a single value of layer thickness from a 2D slice of a 3D particle, as with SEM measurements, the ability to accurately characterise layer thickness variations across a 3D volume serves as both an excellent baseline measurement before corrosion or irradiation testing and can serve to validate alternative techniques.

Furthermore, layer thickness within the particle is particularly important to the understanding of the following mechanical failure mechanisms:

1. Kernel migration induced by thermal gradients.
2. Effect of dimensional changes in the IPyC layer upon the SiC failure.
3. Pressure induced failure of the SiC layer due to FP and CO build-up during operation.
4. Debonding of SiC and IPyC at their interface during irradiation.
5. OPyC failure due to dimensional changes induced by irradiation.

Variations in layer thickness can adversely affect the TRISO particle properties in service, by introducing deviations from sphericity, leading to unsymmetrical heat gradients across the particle which can cause kernel migration. The so called “amoeba effect” [9,10] induces migration of the UO_2 kernel along the thermal gradient. If the kernel comes into direct contact with the SiC, it will induce corrosion, which can ultimately lead to particle failure and the release of fission products.

Both radiographs and XCT have been used previously to measure layer thicknesses [11], however the precise determination of the layer boundaries due to resolution and material attenuation has proven a consistent problem. The use of phase contrast [5] combined with high resolution instruments can be used to clearly define the TRISO layer boundaries, while the use of appropriate filters [6,11] such as those used in this study can be used to amplify this effect to simplify the data post processing.

Unfortunately due to the high density of the kernel compared to the graphite and SiC layers the tomogram from the VersaXRM displays some beam hardening as illustrated in Fig. 2a. The effect of the beam hardening makes the automated segmentation of the TRISO layers in 3D very challenging. To distinguish between pores and pyrolytic carbon an anisotropic diffusion filter was applied. The filter acts to remove noise while preserving edge features. To

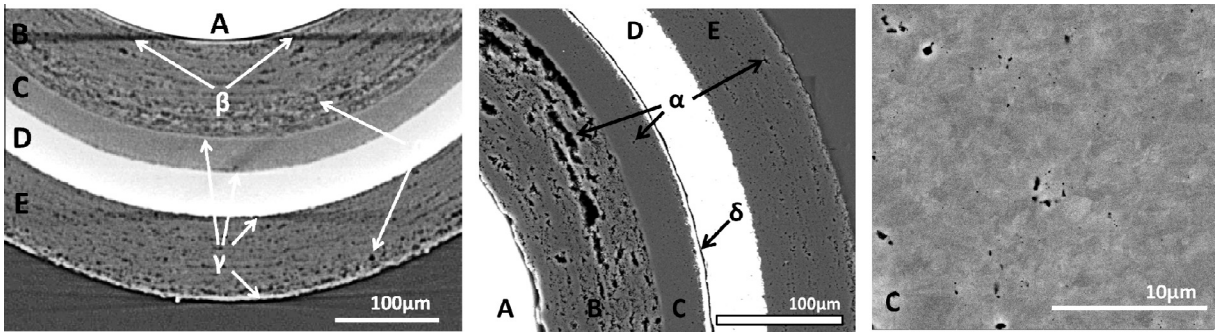

Fig. 2. Magnified regions of interest of the TRISO particle from (a) the VersaXRM tomograph and (b) SEM. **α** shows porosity in the Buffer, IPyC and OPyC layers, **β** shows the beam hardening effect from the denser kernel, **γ** shows the phase contrast effect around each layer, **δ** shows the crack produced in the SiC layer during SEM preparation, (c) higher magnification SEM micrograph of the SiC layer showing pores below 3 μm.

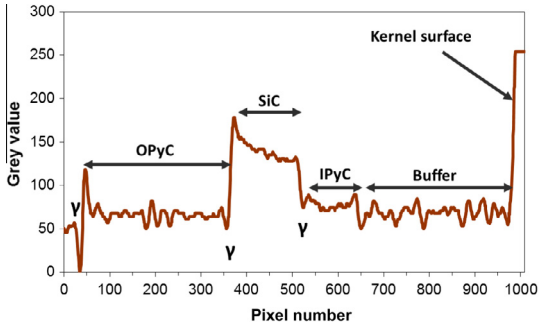

Fig. 3. Grey scale profile across a TRISO particle as shown in Fig. 2a. Each pixel equates to 0.56 μm. **γ** shows the phase contrast effect obtained for the specimen at the layer interfaces.

segment the porosity in each layer, adaptive thresholding was applied followed by manual corrections of the segmented volumes where necessary in order to correct the streaking artefacts from the kernel. Fig. 3 demonstrates the typical variation in grey scale values from the surface of the kernel to the outside edge of the OPyC. The TRISO particle data from the VersaXRM also displays a significant in-line X-ray phase contrast effect [12] particularly at the surface of the TRISO particle (Fig. 3). This phase contrast effect is manifested as an edge-enhancement and is particularly useful in aiding automatic segmentation of features when the material weakly absorbs the hard X-rays produced by typical laboratory sources. Figs. 2a and 3 show that the phase contrast effect clearly defines the boundaries between different TRISO layers. However, excessive phase contrast can obscure features having a similar length scale to the edge contrast [12].

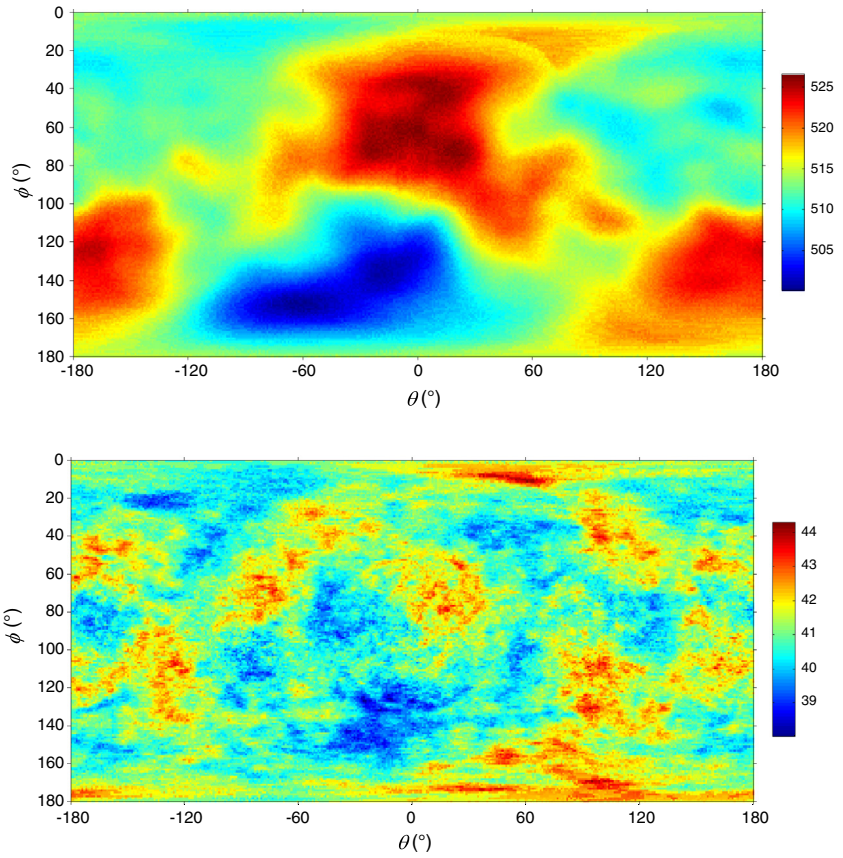

Fig. 4. (a) A map of the kernel diameter (in microns), where ϕ and θ represent the polar (ϑ) and azimuthal (φ) angles. (b) Profile map of the IPYC layer thickness (in microns).

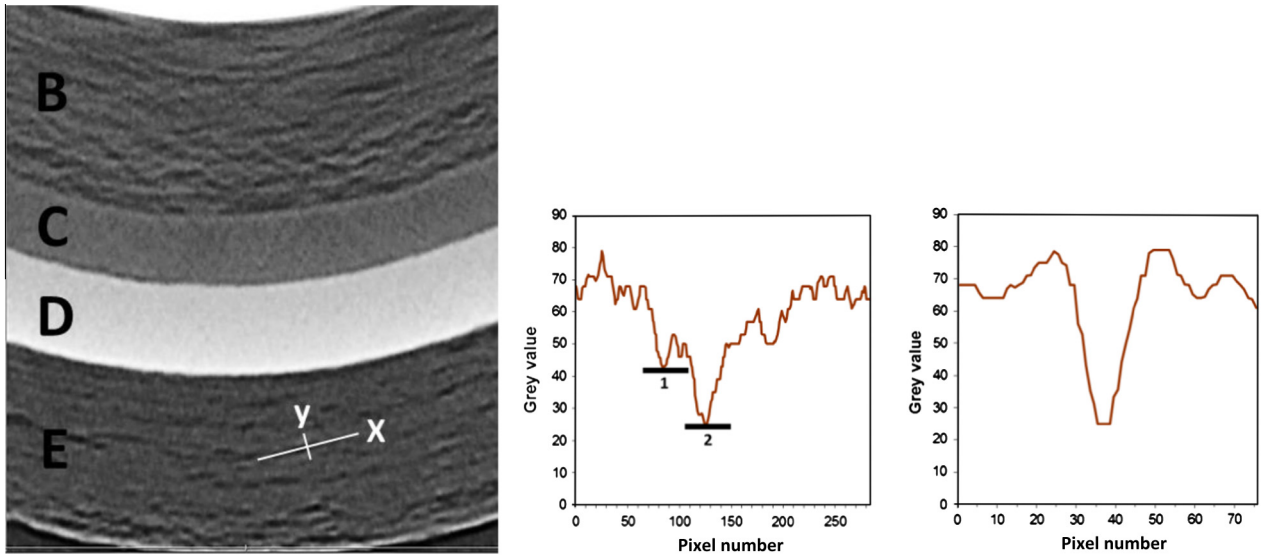

Fig. 5. (a) Example of the Xradia VersaXRM slice showing the Buffer (**B**), IPyC (**C**), SiC (**D**) and OPyC (**E**) layers, (b and c) grey scale profile across a pore as indicated by **X** and **Y** in (a). Each pixel equates to 0.56 μm. **1** shows the typical grey scale profile seen for pixels that partially cover pore and matrix, while **2** is the typical grey scale profile observed pixels that are completely covered by the pore.

To calculate the layer thicknesses the difference in radial distance from the particle centre to the inner and outer edges of each layer were determined for a range of polar (ϑ) and azimuthal (φ) angles for 129,600 radii drawn from the centre of the TRISO particle covering the whole 4π steradians using in house MATLAB software (Table 1). To compare the different TRISO layers the data were then displayed as two dimensional profile maps (Fig. 4a and b). These profile maps can then be used to understand the impact of layer thickness variations upon the deposition of subsequent layers during the particle formation.

Variations in layer thickness imply a deviation from uniform layer thickness early in the fabrication process which could potentially lead to larger effects in the outer layers. Such deviations from sphericity are bad, but tolerable to a point. X-ray CT has the advantage over conventional wide field optical examination as the source of the mis-shapeness can be identified from the kernel towards the shell.

3.3. Quantifying pore morphologies

Unfortunately an analysis of the respective pore structures within the OPyC and buffer layers is not straightforward due to the combined effect of the beam hardening from the highly attenuating kernel (Fig. 2a) and the resolution limit (0.7 μm) of the Xradia Versa instrument. An example of the partially filled voxel effect due to the resolution limit is demonstrated in Fig. 5 and is explained in more detail by Maire and Withers [13]. The effect seen in Fig. 5a–c is not what we would traditionally associate with the partial volume effect since the features occur over tens of microns. This indicates that these regions contain a porous type structure below the resolution limit, thus resulting in the partial volume effect. Therefore although the pore structure appears relatively large as shown in Fig. 5a, the reality is that a large proportion of these large pores are composed of a much finer and closely packed pore structure as indicated by Fig. 5b. This makes the identification of exact pore diameter and length difficult to ascertain. From the Versa data it is impossible to determine whether the structure within these areas is composed of either isolated or interconnected pores, however the higher resolution data presented in Section 3.4 shows that these fine pores are in reality interconnected.

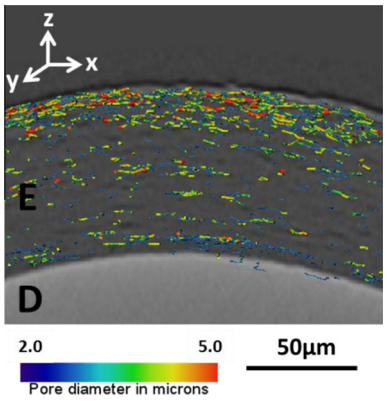

Fig. 6. (a) Xradia VersaXRM Orthoslice showing the SiC (**D**) and OPyC (**E**) layers with the pore volumes superimposed. Pore diameter is colour coded to identify large pore clustering.

In view of the difficulty in segmenting the porosity due to the beam hardening artefacts, an adaptive thresholding [13] technique was used. Further the volume analysed was increased from 50% for the buffer layer to 100% for the OPyC layer. The segmented pore volumes of the buffer and OPyC layer were visualised in Avizo (Fig. 6). In order to obtain a better understanding of the pore interconnectivity and volumes were analysed with a skeletonization/medial axis transform in which an object is represented by a path along its centre and the associated thickness at each point on the path in order to distinguish between the larger and smaller pores. The skeletonized network was combined with the visualized pore surfaces to allow both the pore interconnectivity and the pore size distribution to be compared visually as shown in Fig. 6. The skeletonised pore data was then used to extract the local pore diameter values and lengths as shown in Fig. 7. The distribution of the pores in the buffer and OPyC layers are summarised in Fig. 7. In both cases the pores are snakelike and ranged from a few microns up to 260 μm and 1300 μm in length in the buffer and OPyC layers respectively. From this it is evident that both layers have pores with a fairly narrow range of diameters but a much more significant spread of pore lengths, with the OPyC pores being slightly thicker and slightly shorter than those in the buffer layer.

Although the vast majority of pores in the buffer are less than 30 μm there are a small number of pores that are much longer

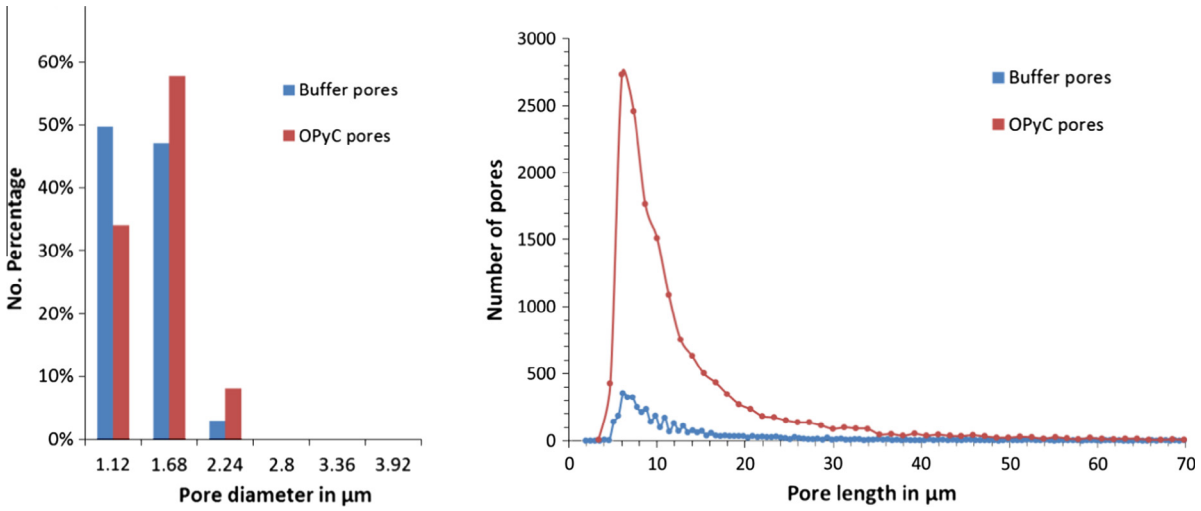

Fig. 7. (a) Graph showing the percentage of pores in the buffer and OPyC layers against the local diameter of the pores. The mean pore diameter was 1.4 μm and 1.5 μm from a total of 788,000 and 3,593,000 measurements for the buffer (4450 individual pores) and OPyC (15334 individual pores) layers respectively. (b) Graph showing the number of pores in the buffer and OPyC layers against the pore length. The mean pore length was 15.7 and 14.6 μm for the buffer and OPyC layers respectively. Pore data accounted for 50.5% and 100% for the buffer and the OPyC layers respectively.

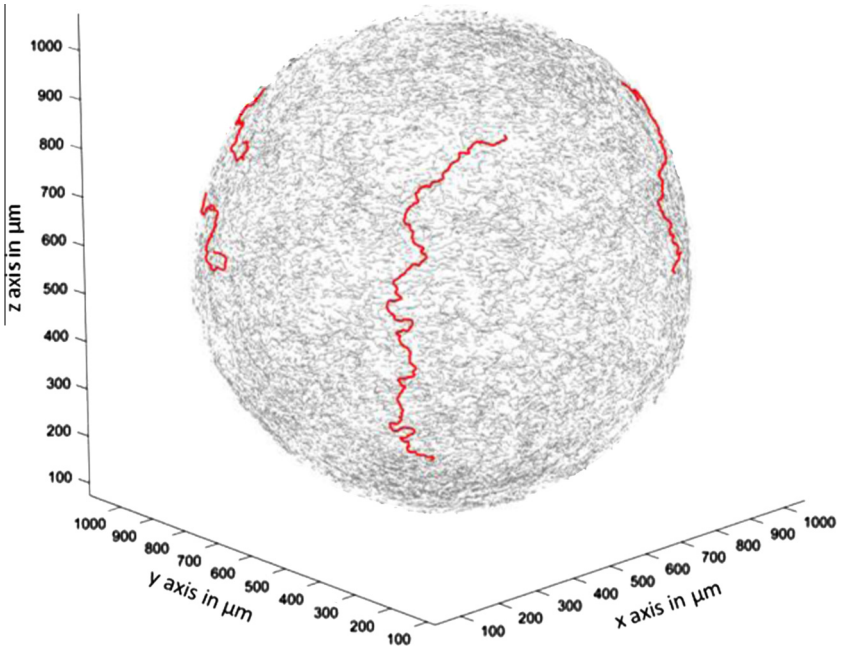

Fig. 8. A three dimensional volume of the pore skeletonised data in the OPyC layer. Pores over 1000 μm are illustrated in red. Units on the *x*, *y* and *z* axis are in microns. (For interpretation of the references to colour in this figure legend, the reader is referred to the web version of this article.)

which appear to be randomly dispersed throughout the buffer layer (see Fig. 8). The existence of such an interconnected pore structure will have an interesting effect upon the absorption and diffusion of fission gasses from the kernel and into the buffer. In this case the existence of interconnected pores might significantly increase the redistribution of the gasses throughout the buffer layer, potentially preventing localised pressure increases within the layer. These pores are unlikely to cause significant issues with the diffusion of fission products to outer layers, as there is very limited large radial porosity, although at the smallest length scales small radial pores become evident, crosslinking the circumferential porosity. The pore morphology and distribution within the buffer layer will also affect the thermal gradient [14].

3.4. High resolution CT pore imaging

The pores in the OPyC layer were also viewed at higher resolution using the ULTRA CT. Due to the higher magnification the volume fraction of the OPyC layer analysed is 0.077%. Other layers were not so easy to access at 8 kV due to the poor X-ray penetration of the SiC layer. Xradia ULTRA pore data is less vulnerable to the partial volume effect, and shows essentially no beam hardening artefacts[1] which makes the segmentation of the

[1] The significantly reduced beam hardening effect can be expected due to the poor absorption characteristics of graphite and the Ultra using a very narrow range of X-ray energies centred on 8.1 keV.

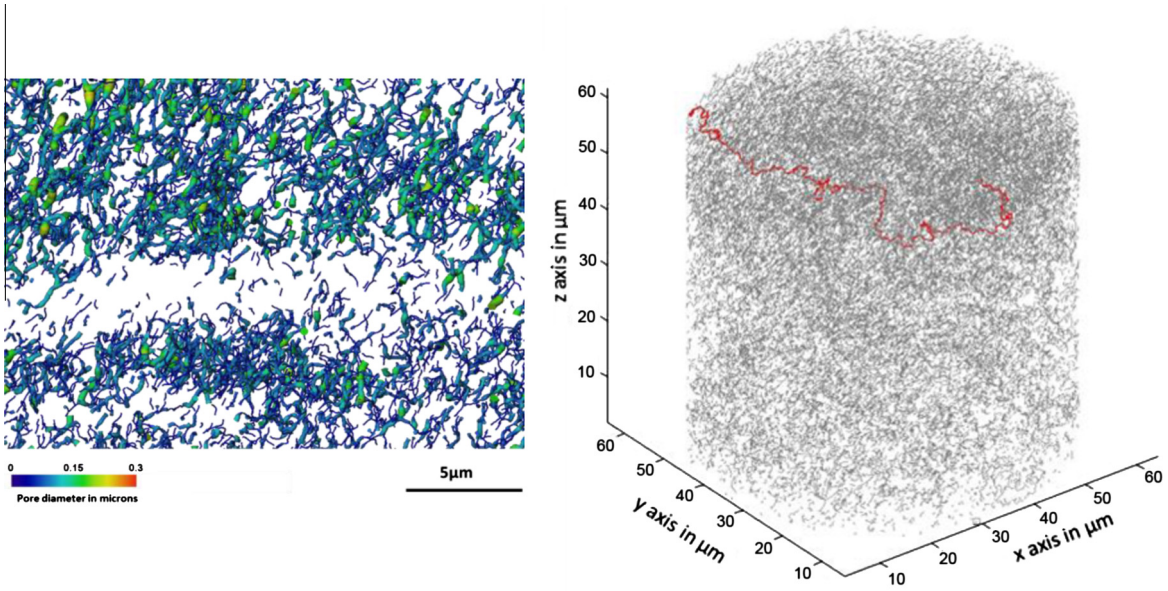

Fig. 9. Pore skeletonisation and size distribution for the OPyC layer for the Xradia Ultra XRM data. Images show the *z* axis perpendicular to the particle surface. (a) Shows pores that are orientated perpendicular to the layer surface and result in porosity bridging high porosity regions shown in Fig. 6. (b) Total pore volume analysed with the largest interconnected pore of 190 µm in length.

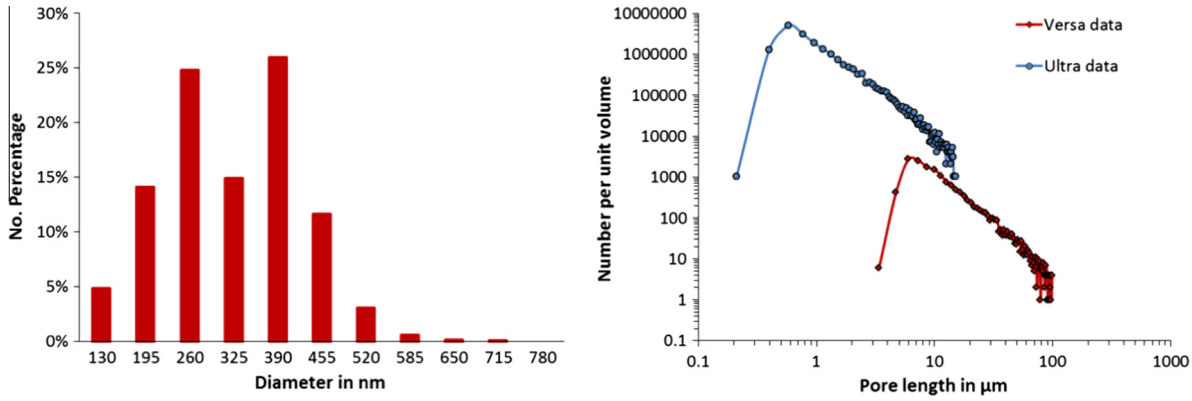

Fig. 10. (a) Graph showing the percentage of pores in the OPyC layer against the local diameter of the pores. Pore data for the OPyC layer was collected on the Xradia ULTRA instrument with data resolution of 65 nm for a respective volume of 862,760 µm^3 containing 18,400 individual pores. (b) Graph showing the number pores per unit volume in the OPyC layer against the local length of the pores.

pores straight forward. Using Avizo's quantification module the segmented pore volume accounted for 3.4% of the OPyC volume measured, which is larger than the data obtained on the Versa instrument (2.4%) but can be attributed to the higher resolution picking up smaller pores. The pore volume was skeletonised and displayed with the pore surface as shown in Fig. 9. In Section 3.3 the pore morphologies formed concentric planes along the layers, however the higher resolution data (Fig. 9a and b) shows that the pores are also formed radiating away from the centre of the pore, although this is unlikely to be problematic, due to the limited role the layers play in fission product containment.

As described above the skeletonised pore data was then used to extract the local pore thickness values and lengths as shown in Fig. 10a and b. If the number of pores per volume is considered (Fig. 10b) for the entire OPyC layer then it can be seen that the majority of pores are below the resolution of the Versa instrument. This explains the increase in percentage volume porosity as well as exposing the highly complex pore morphology. As explained above the function of the OPyC layer is to act as a barrier against fission product release in the event of a defective SiC layer, the presence of large interconnected pores in the OPyC layer renders it ineffective. Even if these large pores tend to occur in specific layers as previously discussed the presence of sub-micron pores as detected by the Xradia Ultra instrument shows that the large pores are connected across the layers by finer pores that run perpendicular to the kernel surface. This interconnected pore structure means that any fission product passing through a damaged SiC layer will have a multiple paths through the OPyC layer. Further analysis of Fig. 10b shows that although the spacial resolution of the Zeiss Xradia VersaXCT data is 0.7 µm in reality the identification of pores is only possible above 3.0 µm. By comparison the spatial resolution of the Xradia Ultra data is 150 nm and the true identification of pores is only possible above 500 nm. By comparing pore length via multi scale imaging techniques (Fig. 10b) it can be seen that the proportion of pores increases as pore length decreases at the same relative rate between both resolutions. The discrepancy of the Xradia Versa data showing a lower proportion of pores could be attributed to either the thresholding technique explained in

Fig. 5b where a conservative threshold was used to avoid the inclusion of partial volume effects, or the fact that the higher resolution data represents only a small volume of the entire OPyC and may therefore be unrepresentative.

4. Conclusions

The results presented here illustrate how recent advances in laboratory based X-ray CT instruments allow the examination of surrogate TRISO particles at the nano and micro-scales in 3D. In this case study high resolution X-ray CT has been shown to be a viable tool in profiling the TRISO particles in two important aspects; the first is as a tool to characterise the individual TRISO layers with variations in thickness and their subsequent interactions, allowing manufacturing validation as well as assisting in working towards a mechanistic understanding of fabrication and in-service issues. In addition a wide variety of studies comparing irradiation induced creep or shrinkage to the pristine particle is now possible. The second important aspect is in the three dimensional visualisation and numerical characterisation of the pore structure for both the buffer and OPyC layers. Such observation has not been possible up until now due to the limitations on imaging imposed by SEM sample preparation. A detailed understanding of the TRISO pore network may yield clues to to fission product retention failure mechanisms, potentially leading to improvements in particle structure and performance.

Due to the resolution limits related to the field of view a multi scale analysis is essential to the true characterisation of the pore networks. In this study the micro scale analysis showed the coarse pore structure over the entire particle as well as individual layer information. However nano scale X-ray CT revealed the true extent of the pore interconnectivity. In this study the numerical analysis of the pore network correlated well between the two scales allowing a better understanding of the complete TRISO pore structure. In essence the 50 nm, nano-, and 1 μm resolution, micro-computed tomography (CT), have been able to quantify non-destructively porosity at the 0.3–10 μm and 3–100 μm scales respectively. This indicates that pore distributions can reliably be measured down to a size approximately 3 times the pixel size which is consistent with the segmentation process employed. Future work could also combine SEM analysis of the pore networks at higher resolution in order to produce a far more in depth characterisation utilising a correlative approach [15].

The ability to non-destructively observe the pore structure throughout the particle in 3D, as well as extract valuable numerical data is a significant advantage over the traditional use of SEM microscopy. This has been directly shown by the identification of pores that can extend over hundreds of microns, which have not been reported previously. In addition X-ray CT has demonstrated that SEM sample preparation can introduce significant new porosity. If SEM analysis is to remain the standard characterisation technique for nuclear fuels then micro X-ray CT may offer a viable validation method to optimise specimen preparation procedures to minimise the introduction of defects during preparation.

Although XCT has great potential as a characterisation technique that offers both a non-destructive advantage over SEM analysis as well the 3D capabilities it does have certain limitations. Most significantly, the beam hardening effect which at present makes the automated characterisation of the pore structures very difficult, this problem will be more pronounced when imaging uranium bearing materials. Another issue arises from the optimum accelerating voltage utilized for the more X-ray attenuating kernel compared to the surrounding layers. In the case of uranium the high accelerating voltage required for imaging the kernel would mean that the outer layer would display a very poor contrast. However with the continuing advances in X-ray source's, the development of multi energy scanning techniques as well as visualization software development it is likely that these issues will be overcome in the near future. Problems associated with the limited field of view as resolution increases can be resolved by taking overlapping scans and then stitching data sets together [16], this however can be a time consuming process.

Despite these limitations XCT has been shown to be a viable tool for the characterisation of TRISO particle microstructure. At synchrotron facilities TRISO particle analysis could take tens of minutes, while the monochromatic beam would eliminate the beam hardening artefacts previously described. The analysis of TRISO particles on laboratory instruments presently takes 10 h however with improved X-ray sources, detectors and reconstruction algorithms this is likely to be reduced to around 1 h or less. For both XCT acquisition techniques the visualisation and quantification stages are the most time consuming steps, however as described above improved algorithms should a fully automated process that would take less than an hour per dataset. The described techniques could in principle be applied to temporal (time lapse) studies to understand the relationship between processing conditions and final microstructure and to validate models of degradation. One area of interest would be the in-situ crush testing of irradiated vs virgin material at low and high temperatures (up to 1600 °C), this information could then be applied to accident simulations. In addition these results could then in turn be used to influence TRISO particle manufacturing.

Acknowledgements

Scanning and analysis was performed at the Henry Moseley X-ray Imaging Facility which has been funded through support from EPSRC under Grants EP/F007906, EP/F028431 and EP/I02249X. Imaging on the UltraXRM-L200 system was carried out at Zeiss Xradia Inc., Pleasanton, CA, USA.

References

[1] E. López-Honorato, P.J. Meadows, J. Tan, P. Xiao, J. Mater. Res. 23 (6) (2008) 1785–1796.
[2] R. Kirchhofer, J.D. Hunn, P.A. Demkowicz, J.I. Cole, B.P. Gorman, J. Nucl. Mater. 432 (1–3) (2013) 127–134.
[3] S. De Groot, P. Guillermier, K. Sawa, J.-M. Escleine, S. Ueta, V. Basini, K. Bakker, Y.-W. Lee, M. Perez, B.-G. Kim, Nucl. Eng. Des. 240 (10) (2010) 2392–2400.
[4] D. Rochais, G. LeMeur, V. Basini, G. Domingues, J. Eng. Des. 238 (11) (2008) 3047–3059.
[5] W.-K. Kim, Y.W. Lee, M.S. Cho, J.Y. Park, S.W. Ra, J.B. Park, Nucl. Eng. Des. 238 (12) (2008) 3285–3291.
[6] M. Yang, J. Zhang, S.-J. Song, X. Li, F. Meng, T. Kang, W. Liu, D. Wei, NDT E Int. 55 (2013) 82–89.
[7] A.C. Slaney, M. Slaney, Principles of Computerized Tomographic Imaging (Classics in Applied Mathematics), Society for Industrial and Applied Mathematics, 1987.
[8] A. Kyrieleis, V. Titarenko, M. Ibison, T. Connelly, P.J. Withers, J. Micros. 241 (1) (2011) 69–82.
[9] R. Konings, Comprehensive Nuclear Materials: Basic Aspects of Radiation Effects in Solid/Basic Aspects of Multi-Scale Modeling, Elsevier Science, 2012.
[10] M. Wagner-Löffler, Nucl. Technol. 35 (2) (1977) 392–402.
[11] W.-K. Kim, Y.-W. Lee, S.-W. Ra, Int. J. Inform. Process. Syst. 1 (1) (2005) 36–40.
[12] R. Bradley, A. McNeil, P.J. Withers, Proc. SPIE 7804 (780404) (2010).
[13] E. Maire, P.J. Withers, Int. Mater. Rev. 54 (1) (2014) 1–43.
[14] A. Krach, S.G. Advani, J. Compos. Mater. 30 (8) (1996) 933–946.
[15] T.L. Burnett, S.A. McDonald, A. Gholinia, R. Geurts, M. Janus, T. Slater, S.J. Haigh, C. Ornek, F. Almuaili, D.L. Engelberg, G.E. Thompson, P.J. Withers, Sci. Reports 4 (4711) (2014).
[16] A. Kyrieleis, M. Ibison, V. Titarenko, P.J. Withers, Nucl. Instr. Meth. Phys. Res. A 607 (3) (2009) 677–684.